Locating liquid-solid transitions in computer simulations based on local structure analysis

1993 J. Phys.: Condens. Matter 5 8509

(http://iopscience.iop.org/0953-8984/5/45/003)

J. Phys.: Condens. Matter 5 (1993) 8509–8522. Printed in the UK

Locating liquid–solid transitions in computer simulations based on local structure analysis

A C Mitus†, D Marx‡||, S Sengupta‡, P Nielaba‡, A Z Patashinskii§ and H Hahn†

† Institut für Theoretische Physik, TU Braunschweig, Mendelssohnstrasse 3, D-38106 Braunschweig, Federal Republic of Germany

‡ Institut für Physik, Universität Mainz, KoMa 331, D-55099 Mainz, Federal Republic of Germany

§ Northwestern University, Department of Physics and Astronomy, 2134 Sheridan Road, Evanston, IL 60208, USA

Received 9 August 1993

Abstract. The concept of local structure in fluids is applied to a complex model fluid with classical translations in two dimensions and two internal quantum states. We demonstrate the usefulness and efficiency of an analysis based on local structure parameters that allows us to locate the liquid–solid transition density from configurations generated by standard constant-volume simulations. Our findings are in close agreement with recent predictions from a density-functional treatment of this freezing transition. In addition to these methodological aspects, open questions concerning the conjectured existence of two triple points in the two-dimensional fluid with internal quantum states can be settled.

1. Introduction

Since the introduction of computer simulation methods, the investigation of phase transitions in the necessarily small finite systems is a challenging problem in statistical physics. One approach consists in computing *thermodynamic* functions as equations of state or free energies via thermodynamic integration. A wealth of impressive work along these lines has been done for simple fluids [1]. Among such methods for liquid–solid transitions we mention the 'artificial-solid method' [2] and the Frenkel–Ladd method or modifications thereof, see [3] for a recent application and further references. Another more recently exploited approach consists in extracting *directly* from the *microscopic* simulation data relevant information leading to the location of phase transitions. Some progress concerning the liquid–gas transition became possible with the introduction of the Gibbs-ensemble [4] method and the finite-size block analysis technique for off-lattice [5–7] models. However, neither method is ideally suited for investigating liquid–solid transitions. The Gibbs-ensemble method is hampered by the usual 'particle insertion problem' known from grand canonical simulations [8] of dense fluids, while on the other hand the block analysis cannot (in general) resolve the small density differences between liquid and solid phases [6].

The key idea of the present method for the location of liquid–*solid* transitions consists in using only *microscopic* simulation data, i.e., *configurations*, which is similar in spirit to the

|| Present address: IBM Research Division, Zurich Research Laboratory, Säumerstrasse 4, CH-8803 Rüschlikon, Switzerland.

0953-8984/93/458509+14$07.50

above methods used for liquid–*gas* transitions. Since we have to distinguish liquids from solids, there are two basic concepts that may be suited. The classification of configurations along the lines of Voronoi polyhedra or their dual, the Delaunay polyhedra, has already been widely used for the investigation of melting and nucleation, see, e.g., [9] and [10], but only recently for the determination of the liquid–solid transition [11]. The idea of local invariants [12–17] was also mainly used to investigate in detail microscopic structures of fluids. Recently, one specific set of order parameters, the global bond-order parameters [13], was used to estimate free-energy barriers in crystal nucleation [18]. In connection with two-dimensional (2D) melting [19] and the search for the hexatic phase, an analysis of nearest-neighbour bond-angular susceptibilities on various length scales has been performed [21]. In the present paper, we use 'fluctuating distributions' of *local* invariants to estimate the location of the liquid–solid transition in a given parameter space. We will demonstrate that this method is extremely useful in locating liquid–solid transitions in simulations with constant volume. The method is not designed to yield high-precision data. However, it is well suited for rough investigations of liquid–solid transitions over a wide range of control parameters in 'expensive' fluid models.

We apply our ideas to the now well studied fluid with internal quantum states, see [20], [6], [7] and [22]. This system was recently extensively investigated in 2D using path-integral Monte Carlo (PIMC) methods [23] in combination with the block analysis method [6]. The phase diagram, as found in the simulations, includes fluid, gas, liquid and *square solid* phases combined with ferromagnetic and paramagnetic ordering of the internal quantum states. In order to understand the occurrence of the *square* solid phase, the system was investigated [22] with the density-functional theory (DFT) of freezing generalized to handle liquids with internal quantum states. This revealed the possible existence of the expected *hexagonal* solid phase in addition to the discovered square solid phase, resulting in two triple points. In addition, it was possible to obtain the *complete* phase diagram in the temperature–density plane. In the present paper, we return to simulations and investigate from this standpoint the liquid–*hexagonal*-solid transition in this complex fluid. Since simulations of such many-body quantum systems are very time consuming, only *efficient* analysis methods can be used with a chance of success; the mapping of the gas–liquid and gas–square-solid coexistence lines in [6] was only possible due to methods especially tailored to the problem. The usefulness of the analysis based on the concept of local structures for the location of the liquid–solid transition is demonstrated by comparing it to DFT results.

The organization of the rest of the paper is as follows: we start by introducing our method to analyse the liquid–solid transition in section 2, followed by the definition of the model Hamiltonian in section 3. The PIMC simulations are briefly described in section 4.1, and the theoretical treatment using a mean-field (MF) approximation and DFT is given in section 4.2. We discuss our results, also with respect to similar work by other groups, in section 5, and close this paper in section 6 with a summary of our main results.

2. Local structure analysis

Before going into the details, we first sketch the basic ideas behind the approach. The concept of local order parameters [12–17] seems to be an ideal starting point for the location of liquid–solid transitions based directly on configurations. Based on these quantities, our central idea is to decompose a given configuration into patterns of typical *local* structures, where a local structure consists, loosely speaking, of a few-atom cluster. In case of a 2D liquid of point particles, typical clusters consist of 6 ± 1 neighbours around a central

particle. The low-temperature/high-density phase, termed 'solid' from now on (see [19] for reviews of the 2D melting problem), consists of mainly hexagonal clusters centred around sixfold-coordinated particles with a certain equilibrium density of defects, i.e., vacancies and interstitials. This defect concentration (of typically only a few percent in the solid) increases dramatically in the liquid [11], effectively leading to a sizable concentration of clusters centered around five- and sevenfold-coordinated particles. In addition, the relative angles connecting the central particle with its neighbours start to deviate from their average values in the solid phase. The *thermal displacements* of the particles constituting the clusters are taken into account as Gaussian *fluctuations*, where the mean square displacement of the fluctuations has to be determined in the analysis and yields an estimate for the Lindemann parameter. Thus, if a configuration deep in the solid state is decomposed into ideal local structures, only fluctuations of hexagonal clusters with corresponding relative angles contribute significantly to the overall structure. In the liquid state, however, the defect clusters become important, i.e., large deviations of the relative angles occur. Contrary to methods based on Voronoi decompositions [9–11], only rotationally invariant angular features are exploited in the present approach in the form of the local invariants.

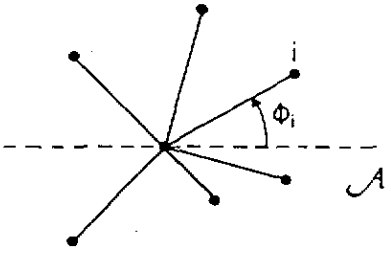

Figure 1. Schematic picture of a seven-atom cluster around a central atom at r with definition of the angle ϕ_i.

We characterize the local structures by structural invariants [17]. In this approach we describe the local order in the 2D liquid in the vicinity of an atom located at point r, see figure 1, by the 2D *local* version of the bond-order parameter [13]

$$Q_{lm}(r) = \frac{1}{N_0}\sum_{i=1}^{N_0} Y_{lm}(\theta_i, \phi_i) \tag{1}$$

where Y_{lm} denotes spherical harmonics and the sum is over the N_0 neighbours of atom r; the pair of angles (θ_i, ϕ_i) fixes the direction between the central atom and the ith neighbour in some space-fixed coordinate frame. In 2D the atoms lie in a plane that we chose to be perpendicular to the $\hat{z}$ axis of the coordinate frame, i.e., all θ_i are equal to $\frac{1}{2}\pi$, and ϕ_i is measured relative to some axis $\mathcal{A}$. In (1), we always consider the $N_0 = 6$ nearest neighbours. In order to obtain a rotationally invariant expression, the axis dependence has to be summed over and we use [13, 10, 17]

$$Q_l^2(r) = \frac{4\pi}{2l+1}\sum_{m=-l}^{l} |Q_{lm}(r)|^2. \tag{2}$$

Systems with hexagonal solid structure can be analysed via [17] the invariant Q_l with $l = 6$, referred to as the *local structure parameter*; for convenience we from now on omit the subscript l. In contrast to other approaches [18], the following analysis will be based

directly on the probability density function $\rho(Q)$ (referred to as the distribution function from now on) of the *local* structure parameter field $Q(\boldsymbol{r})$ itself, i.e., without defining any *global* structure parameter obtained by averaging $Q(\boldsymbol{r})$ over all bonds in the system [13]. Alternative definitions relying on 2D local structure parameters [24, 19, 21] could also be used. More details on the probabilistic formalism connected with the actual analysis of simulated data and especially the corresponding error estimates can be found in [15–17].

Having defined the local structure parameters, we now consider *fluctuations* of the invariants. Our goal is to decompose the distribution $\rho(Q)$ calculated from MC simulation into what we call the distributions for ideal local patterns Γ_k. The natural choice Γ_6 for a 2D solid is the symmetric seven-atom cluster with a sixfold-coordinated central particle $\boldsymbol{r}$, i.e., the six neighbours $i = 1, \ldots, 6$ form an ideal hexagon. Other patterns $\Gamma_{k\neq 6}$ correspond to non-hexagonal structures and reflect, e.g., the arrangement of particles in the vicinity of dislocations; due to the definition of the N_0 neighbours we only consider seven-atom clusters. The coordinates of the constituent particles can be calculated approximately using the elasticity theory formulae for displacement vectors in the vicinity of a dislocation, see [17]. As already discussed, we expect a 'high concentration' of hexagonal patterns Γ_6 in the solid, whereas other patterns should dominate in the low-density liquid. Since the particles and thus the invariants Q fluctuate (at non-zero temperatures), this effect has to be considered in the analysis. Starting from, say, the hexagonal Γ_6 pattern, we let the six neighbours of the central particle fluctuate according to a Gaussian distribution

$$P_6(\delta\boldsymbol{r}) = (1/\xi_6\sqrt{\pi})\exp[-(\delta\boldsymbol{r})^2/\xi_6^2] \tag{3}$$

where $\delta\boldsymbol{r}$ denotes the displacement vector and ξ_6 its mean amplitude; we measure ξ_6 in units of the distance between the central atom and its neighbours in the regular structure. Using the definition (3), the mean fluctuation amplitude of any atom of the pattern is given by $\xi_6/\sqrt{2}$. The resulting distribution $\rho_6(Q, \xi_6)$ for the Γ_6 pattern degenerates into a delta function for non-fluctuating patterns and smooths out as ξ_6 is increased while the information about the type of pattern is gradually lost. For a fixed fluctuation strength ξ_k, we call these $\rho_k(Q, \xi_k)$ the distributions for *ideal* patterns of the Γ_k type. One can define a measure of the 'structural identity' for such fluctuating patterns [15–17], but we are not going to use this concept here. It turns out [17] that the distributions $\rho_k(Q, \xi_k)$ for seven-atom patterns fall into two classes. One of them consists of $\rho_6(Q, \xi_6)$ alone and the other of non-hexagonal or 'defect' distributions. In other words, the invariant Q distinguishes between hexagonal local structures and any other type of local structure. As a representative of the non-hexagonal distribution we use $\rho_5(Q, \xi_5)$ calculated from fluctuations of a dislocation pattern Γ_5 centred around a fivefold coordinated atom [17]. In figure 2, we present the distributions $\rho_5(Q, \xi_5)$ and $\rho_6(Q, \xi_6)$ for choices of ξ as determined for our model fluid at the transition density for a temperature of $T^* = 0.6$ (see the following sections for details). As essential for the analysis, the hexagonal pattern Γ_6 distribution peaks at a very different Q than that of the defect pattern Γ_5.

Having introduced ideal *fluctuating* patterns, the last step consists in decomposing the distribution $\rho(Q, T^*, \rho^*) = \rho(Q)$ calculated from a simulation at statepoint (T^*, ρ^*). The simplest *ansatz* is a linear superposition of the distributions of the hexagonal Γ_6 and defect Γ_5 patterns

$$\rho(Q, T^*, \rho^*) = c_6\rho_6(Q, \xi_6) + c_5\rho_5(Q, \xi_5) \tag{4}$$

where we have three fit parameters c_6, ξ_6, and ξ_5 ($c_6 + c_5 = 1$) all depending on T^* and ρ^*. The quantity $c_6(T^*, \rho^*)$ is a measure of the 'weight' of the solid phase at statepoint

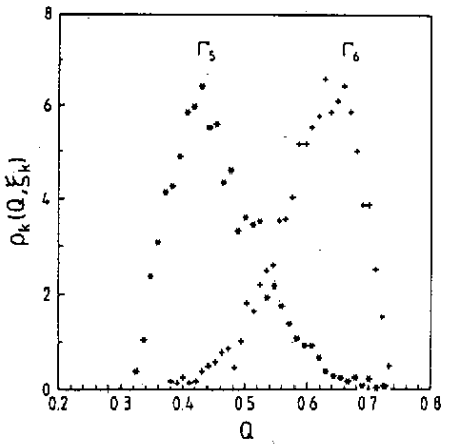

Figure 2. Distributions $\rho_k(Q, \xi_k)$ of hexagonal Γ_6 and defect Γ_5 patterns: crosses, Γ_6 where $\xi_6 = 0.19$; stars, Γ_5 where $\xi_5 = 0.33$.

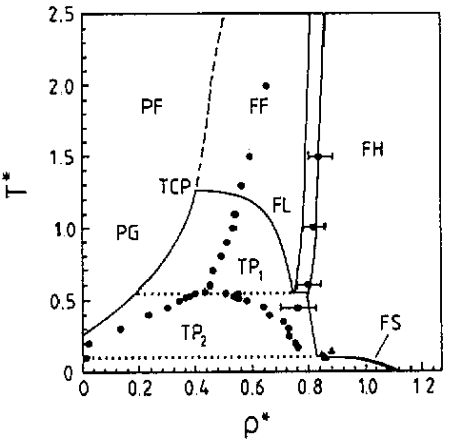

Figure 3. Phase diagram including paramagnetic fluid (PF), ferromagnetic fluid (FF), paramagnetic gas (PG), ferromagnetic liquid (FL), ferromagnetic hexagonal solid (FH) and ferromagnetic square solid (FS) phases. Special points are the tricritical point (TCP) and two triple points (TP_1, TP_2). Curves are MF/DFT predictions (full, first-order transitions; broken, second-order transitions; dotted, triple lines); circles and triangles (FS coexistence densities) are block analysis PIMC data; squares (FH coexistence densities) are local structure analysis PIMC data. For further details see the text.

(T^*, ρ^*): it goes to unity in the deep solid phase and vanishes when approaching the low-density regime. In other words, we can relate c_6 to a 'volume fraction' of the solid phase. Thus, in analogy to the well known lever rule of statistical mechanics, the parameters for which $c_6 \simeq \frac{1}{2}$ should give a *rough* estimate of the coexistence region. Being based on *heuristic* arguments, this criterion should be considered a *rule of thumb* only! A much improved estimate for the criterion can only be obtained after a detailed *quantitative* study of the free energy along the lines of [18] but necessarily including an analysis of associated finite-size effects on the distributions, which is not intended in this exploratory study. The other interesting fit parameter is $\xi_6(T^*, \rho^*)$. Since the mean fluctuation amplitude $\xi_6/\sqrt{2}$ defines the amplitude of the *thermal displacements* of the particles from their regular crystal positions, it should be related to the usual Lindemann ratio. Armed with the parameters c_6 and ξ_6, we can analyse the liquid–solid transition of a specific model on a more quantitative footing.

3. Model fluid with internal quantum states

We model a complex fluid in 2D, which in addition to the translational degrees of freedom also has internal degrees of freedom. The latter can be thought of as quantum-mechanical molecular degrees of freedom coupled to the translations. The mass M of the molecules is assumed to be large enough to allow a classical treatment of the translational degrees of freedom. The molecular centre of mass can take continuous values in a monolayer of area $V = S \times S$. The internal quantum states are represented as simply as possible: to

each molecule we assign a two-level tunnelling system and introduce a distance dependent coupling between the molecular degrees of freedom on different particles. The resulting combined classical/quantum N-particle Hamilton operator of the system reads

$$\hat{H} = \frac{1}{2M}\sum_{i=1}^{N} p_i^2 - \frac{1}{2}\omega_0 \sum_{i=1}^{N} \hat{\sigma}_i^x + \sum_{i<j} U(r_{ij}) - \sum_{i<j} J(r_{ij})\hat{\sigma}_i^z \hat{\sigma}_j^z \tag{5}$$

where p_i and r_i are the momentum and position in 2D of particle i ($r_{ij} = |r_i - r_j|$); $\hat{\sigma}^x$ and $\hat{\sigma}^z$ are the usual Pauli spin-$\frac{1}{2}$ matrices. The potential energy consists of a one-particle (two-level) part and two pair interaction terms $U(r)$ and $J(r)$, where U is chosen to be a hard disk potential for molecules with diameter R and $J(r) = J$ for $R < r < 1.5R$ and zero elsewhere.

These two-state molecules have an internal Hamiltonian $-\frac{1}{2}\omega_0\hat{\sigma}_i^x$ and interact via a pair potential depending on their actual internal state; the hard-disk part is the only remnant of the core–core interactions of the molecules. The important feature of the Hamiltonian (5) is that the interaction term will tend to lift particles out of their internal ground state corresponding to a change of their preferred magnetic state. Due to the distance dependence of the interaction term $J(r)$ the quantum and classical dynamics are non-trivially coupled. Thus a coverage-induced change of the preferred internal quantum state of the molecules is expected as the density is changed. Since the interaction term is short ranged, we expect, roughly speaking, dominance of the one-particle contributions $-\frac{1}{2}\omega_0\hat{\sigma}_i^x$ at low densities, resulting in paramagnetic phases; this is found in case of the gas and low-density fluid phases. As the density is increased, the particles start to feel the interaction term $-J\hat{\sigma}_i^z\hat{\sigma}_j^z$, which induces a ferromagnetic ordering of the internal states; the solid and high-density fluid phases are found to be ferromagnetic. At very high temperatures, only the athermal hard-core contribution is expected to be relevant for phase stability.

The part of the model's phase diagram that is of interest in this investigation is presented in figure 3. The symbols are based on PIMC simulations, and the curves on a combined MF and DFT treatment, see section 4. More features and the experimental background of this particular model, which produces many of the phases found in certain molecular adsorbates [7], can be found in [6] and [7].

4. Simulations and theory

4.1. Path-integral MC simulations and block analysis

The PIMC formalism, see [23] for a general discussion, is most easily described by considering directly the partition function

$$Z(\beta, N, V) = \lambda^{-2N}\frac{1}{N!}\int \mathrm{d}r_1 \cdots \int \mathrm{d}r_N \,\mathrm{tr}_\sigma \exp(-\beta\hat{H}) \tag{6}$$

where the thermal de Broglie wavelength λ results from integrating out the trivial momenta and $\beta = 1/k_B T$ as usual. We use the Trotter formula to discretize the partition function Z in the Trotter dimension P as [20, 6]

$$Z = \lim_{P\to\infty} \frac{A_P^{NP}}{\lambda^{2N} N!} \int \mathrm{d}r_1 \cdots \int \mathrm{d}r_N \sum_{\{S\}} \exp\left[-\beta\left(H_P(\{S\}) + \sum_{i<j} U(r_{ij})\right)\right]. \tag{7}$$

The effective Hamilton function H_P is defined as

$$-H_P(\{S\}) = \sum_{i=1}^{N}\sum_{p=1}^{P}\left(K_P S_{i,p}S_{i,p+1} + \frac{1}{P}\sum_{j=i+1}^{N} J(r_{ij})S_{i,p}S_{j,p}\right) \qquad S_{i,p} = \pm 1 \tag{8}$$

where we have introduced the constants

$$A_P = [\tfrac{1}{2}\sinh(\beta\omega_0/P)]^{1/2} \tag{9}$$

and

$$K_P = (1/2\beta)\ln[\coth(\beta\omega_0/2P)]. \tag{10}$$

The exact quantum properties of the system can now be obtained as thermal averages over the effective *classical* canonical distribution of the $N \times P$ particles

$$\mathcal{P}_{\text{eff}}^{NVT} \propto \exp\left[-\beta\left(H_P(\{S\}) + \sum_{i<j} U(r_{ij})\right)\right] \tag{11}$$

if the required Trotter extrapolation $P \to \infty$ is carried out. Thus, the key is that an N-body (quantum) system could be transformed to a classical system; the price to be paid consists of an increase in the number of degrees of freedom, since we now have an $(N \times P)$-body (classical) problem with $P \to \infty$, and the introduction of more complicated interactions. At this stage, the simulations can be carried out as a standard classical canonical MC simulation using the Boltzmann weight defined in (11). However, it should be noted that, due to the additional degrees of freedom along the Trotter direction, such PIMC simulations are *much* more demanding than simulations of the corresponding classical case.

The liquid–gas coexistence region of the phase diagram is already known from an extensive finite-size block analysis PIMC study [6] of the model. The details of this investigation can be found in [6]; see also [5] for the original papers applying the block analysis to off-lattice models. For the convenience of the reader, we briefly sketch the basic ideas of this method. Consider a fluid in the one-phase region, i.e., well above its critical point. Such a situation is characterized by a number density fluctuating around the average density of the system. For large systems, one can approximate this by a Gaussian density distribution centred around the average density of the system. Well below the critical point, this distribution splits into two branches due to the coexistence of a low- and a high-density phase. Neglecting interfacial effects, this can in turn be approximated by two superimposed Gaussians in the density; the weights are given by the level rule, and the widths depend on the respective compressibilities. Near the critical point, scaling arguments can be used to motivate scaling forms for this distribution function.

The generic system used in computer simulations of fluids consists of a periodic box of fixed shape and box lengths containing a conserved number of particles; in the Gibbs ensemble [4] a skilful combination of ingredients from different statistical ensembles is used, which makes it different in this respect. But even in a system with *constant* volume one can measure density fluctuations if one subdivides the total system by introducing imaginary walls into subboxes or 'blocks' on various length scales. This is the key idea, since one can now measure the average number density of these blocks and actually compute the density distribution function. Finally, the analysis consists of fitting these distributions by Gaussians, which allows one to extract the coexistence densities in two phase regions. Along

these lines, the liquid–gas binodal of our model fluid was mapped. This approach can also be extended to investigate *gas*-solid coexistence as demonstrated in [6] where the *square* solid phase of our model fluid was discovered. The generalization of the block analysis to the liquid–solid transition is (in general) not feasible: the practical implementation of the method relies on the ability to resolve the density difference between the coexisting phases, and in the case of generic *liquid*–solid coexistences this difference is simply too small for tractable system sizes.

In the present study, the PIMC simulations were carried out with the same parameter set ($J = 1$, $R = 1$, $\omega_0/J = 4$) as before [6,22] as a function of dimensionless temperature $T^* = (\beta J)^{-1}$ and density $\rho^* = R^2N/V$. The number N of molecules was again 200 and the Trotter dimension P was chosen such that $P/\beta J \simeq 40$. With this choice of P, the Trotter limit was safely reached [6], as tested by Trotter scaling various observables and comparing the PIMC imaginary time–$\hat{\sigma}^z$ correlation functions with these functions from a virial expansion for low coverages.

4.2. *Mean-field and density-functional theories*

We now sketch the basic ideas of the MF theory [25,20] used to obtain the gas-liquid coexistence boundaries and the paramagnetic–ferromagnetic transitions [20,6]. In addition, it serves as a necessary liquid-state input for the DFT treatment for the liquid–solid transition. The MF treatment of our model closely follows the well known Curie–Weiss theory for the Ising model [26] in a transverse field, with the only difference being that our spins are not restricted to be located on lattice sites. This is approximately modelled by a density-dependent coordination number [25,20] or equivalently an averaged coupling constant J_0

$$J_0 = \rho \int \mathrm{d}r\, J(r) g(r) \tag{12}$$

where as usual $g(r)$ denotes the two-point correlation function for the homogeneous hard-disk fluid. The Helmholtz free energy of the model thus reads in the MF version

$$\beta f(\rho) = \beta f_{\mathrm{cl}}(\rho) + \tfrac{1}{2}\beta J_0 \rho m^2 - \rho \ln\{2\cosh[\beta(J_0^2 m^2 + \tfrac{1}{4}\omega_0^2)^{1/2}]\} \tag{13}$$

where $f_{\mathrm{cl}}(\rho)$ is the free-energy contribution of the non-magnetic part of the Hamiltonian, and within our approximation is simply the free energy of the hard-disk system at the same density. For high temperatures we find a continuous transition from a paramagnetic to a ferromagnetic fluid phase, but below the tricritical temperature T_{TCP} the magnetic transition is accompanied by a (paramagnetic) gas–(ferromagnetic) liquid transition together with jumps in both magnetization and density.

The liquid–solid part of the phase diagram was obtained by combining MF theory for the magnetic transition with DFT for freezing [27]. The basic idea of the Ramakrishnan–Youssouf approach [27] is a second-order expansion of the free-energy functional around its *liquid* state. To include the contribution of the internal quantum states, we start by introducing a combined classical/quantum free-energy functional [22] of the time-averaged number density $\rho(r)$ and the magnetization density $m(r)$ for the Helmholtz free energy. We incorporate the magnetic interaction in the sense of an MF [20] treatment in addition to the non-magnetic hard-disk contribution. The magnetization density is proportional to the number density, i.e., $m(r) = m_s \rho(r)$; we measure the magnetization in the magnetic z direction. In the MF model the magnetic field on one particle due to the interaction with all

other particles is approximated by the average molecular field, $\xi_m(r) = \int dr' m(r-r')J(r')$. The free-energy *functional* in this approximation is finally given by

$$\beta f[\rho] = \beta f_{cl}[\rho] + \frac{\beta}{2}\int \frac{dr}{V} m(r)\xi_m(r) - \int \frac{dr}{V}\rho(r)\ln\{2\cosh[\beta(\xi_m^2(r) + \tfrac{1}{4}\omega_0^2)^{1/2}]\}. \quad (14)$$

The Helmholtz free energies of the solid are obtained by minimization of this functional with respect to both $\rho(r)$ and m_s. Motivated by the simulation results we also studied the *square*-lattice solid in addition to the usual hexagonal solid. Further technical details, such as the choices of the classical contribution $\beta f_{cl}[\rho]$, the direct correlation function and the minimization scheme, are discussed in [22].

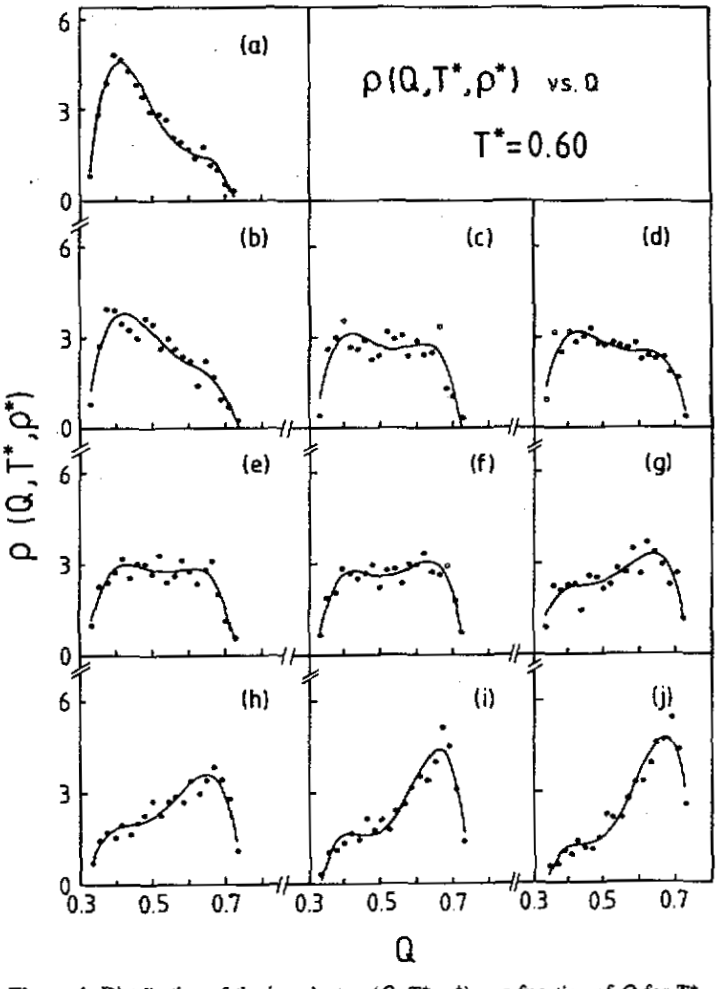

Figure 4. Distribution of the invariants $\rho(Q, T^*, \rho^*)$ as a function of Q for $T^* = 0.6$. The full curves correspond to fits and serve only as guides to the eye. (a) $\rho^* = 0.60$; (b) $\rho^* = 0.70$; (c) $\rho^* = 0.74$; (d) $\rho^* = 0.76$; (e) $\rho^* = 0.78$; (f) $\rho^* = 0.80$; (g) $\rho^* = 0.82$; (h) $\rho^* = 0.84$; (i) $\rho^* = 0.86$; (j) $\rho^* = 0.88$.

5. Results and discussion

We start by showing in figure 4 the raw data of our basic quantity, the distributions $\rho(Q, T^*, \rho^*)$ of the invariants Q at $T^* = 0.6$ for densities covering the range from the liquid to the solid; the fits are useful guides to the eye. These distributions are obtained directly from the configurations as defined in (2). The statistics was improved by averaging six well equilibrated and independent configurations for all densities at $T^* = 0.6$ and 1.0, whereas 12 configurations were used at $T^* = 0.45$ and 1.5. Since we extract only the *local* quantities Q defined by a few nearest neighbours around every particle, each configuration consisting of 200 molecules contains already many independent samples in the sense of a self-average. The data based on 12 configurations give smaller error bars as expected, but in order to improve the statistics considerably, many more configurations have to be analysed during the run. Many more averages are needed if one attempts to obtain more *accurate* data, but as underlined by our results, we have already gathered sufficient statistics with only six configurations in order to *reliably* extract the quantities of interest.

The distributions in figure 4 in general have a two-peak structure, which indicates the existence of at least two types of local order. One can clearly see a qualitative change in the shape of the distribution as the density is increased: the low-density regime is dominated by a peak at $Q \simeq 0.4$, whereas high-density configurations have a prominent peak at the hexagonal value of $Q \simeq 0.65$. It is important for the analysis to note that the *positions* of the peaks do not change as the density is increased, only the relative *weight* of the two contributions is density dependent. Thus we can see *qualitatively* that the local structure of the fluid, as characterized by its bond-order parameter *distribution*, changes noticeably as a function of density.

The next step of the analysis consists in obtaining a *quantitative* estimate for the crossover density. A rough estimate can be obtained by inspection of the distributions of the invariants in figure 4; it must be located somewhere in the region $\rho^* = 0.76$–0.80 at a temperature of $T^* = 0.6$. Its quantification follows from the decomposition (4) of the simulated distributions $\rho(Q, T^*, \rho^*)$ into hexagonal $\rho_6(Q, \xi_6)$ and non-hexagonal $\rho_5(Q, \xi_5)$ distributions. This decomposition is a fit with the three free parameters ξ_6, ξ_5, and c_6 yielding the relative weight of hexagonal local structures and corresponding fluctuation strength of the patterns.

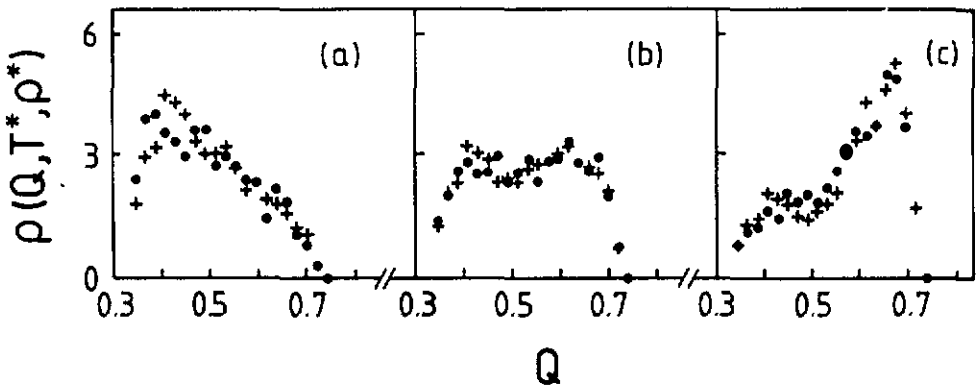

Figure 5. Decomposition of distributions of the invariants in fluctuating hexagonal Γ_6 and defect Γ_5 patterns as a function of Q for $T^* = 0.6$: circles, simulation data $\rho(Q, T^*, \rho^*)$; crosses, decomposed data using (4). (a) $\rho^* = 0.70$; (b) $\rho^* = 0.80$; (c) $\rho^* = 0.86$.

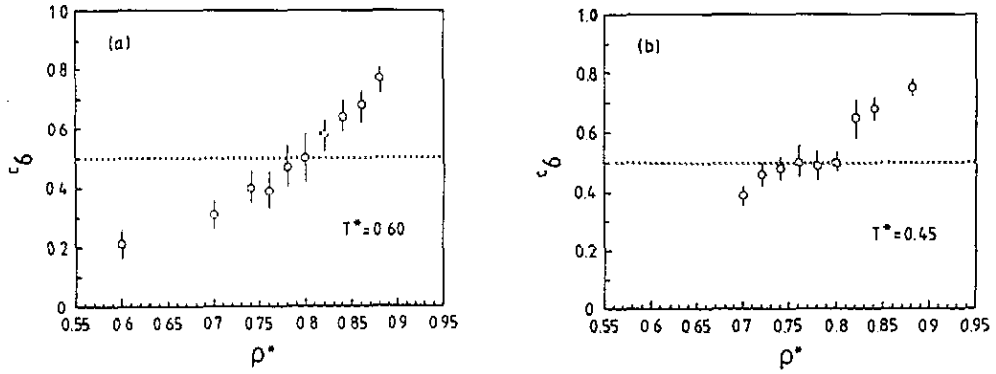

Figure 6. Relative concentration c_6 of fluctuating hexagonal Γ_6 patterns as a function of ρ^*. The dotted line marks $c_6 = \frac{1}{2}$. (a) $T^* = 0.6$; (b) $T^* = 0.45$.

We are now in a position to extract the relative concentration c_6 of hexagonal local structures from the decomposition of the distributions of the invariants $p(Q, T^*, \rho^*)$ obtained for different state points in the (T^*, ρ^*) phase diagram into hexagonal and other local structures. We show such a decomposition for a density corresponding to the liquid, solid and crossover regimes at $T^* = 0.6$ in figure 5. One can nicely see how the superposition of the patterns Γ_6 and Γ_5 fluctuating with the optimized ξ_6 and ξ_5 fits the structures of the fluid in different regimes. The interesting contribution c_6 of hexagonal local structures is plotted in figure 6 for the two temperatures $T^* = 0.6$ and 0.45 as a function of the density; the errors bars are solely based on statistical errors of the local structure analysis. One can clearly see that c_6 increases rapidly from a value of 0.2 (typical of a liquid) at $\rho^* = 0.6$, to 0.8 (typical of a solid) at $\rho^* = 0.88$, which we interpret as an ongoing crystallization of the system upon increasing the density. Since we measure the invariant $Q \equiv Q_6$, this implies that a *hexagonal* solid structure exists at high densities for all the investigated temperatures. As motivated in section 2, we assume that the intersection of the data with $c_6 = 0.5$ gives an estimate of the density ρ^*_{coex} of equal contribution of hexagonal and other local structures. As presented in detail for $T^* = 0.6$ (the curves for $T^* = 1.0$ and $T^* = 1.5$ are qualitatively similar to $T^* = 0.6$), we extracted these densities for four temperatures and plot the data as squares in the phase diagram of our fluid, see figure 3, as obtained from MF and DFT (curves) and previous simulations (circles, triangles). It is rather obvious that the densities ρ^*_{coex} are good estimates of the coexistence region of the liquid with the hexagonal solid. Having systematic errors such as, e.g., neglect of the non-vanishing vacancy and interstitial concentrations of equilibrium solids [28] and of course finite-size effects [21], the accuracy of the proposed method should not be overestimated. Especially when approaching the liquid–gas coexistence line for $T^* = 0.45$, the data in figure 6(*b*) contain a lot of scatter, probably because of large interfacial effects and gaseous contributions in the configurations. Nevertheless, we can estimate directly from the simulation how the liquid–hexagonal coexistence line reaches the liquid–gas binodal. This is now the demonstration by simulation that the DFT prediction of a *second* triple point (TP_1 in figure 3), with coexistence of paramagnetic gas, ferromagnetic liquid and ferromagnetic *hexagonal*-lattice solid, is qualitatively correct. Only the actual location of this triple temperature is lower: we estimate $T^*_{\text{TP}_1} \simeq 0.35 \pm 0.1$ instead of $T^*_{\text{TP}_1} = 0.55$ from DFT. The triple point TP_2 involving the *square*-lattice solid was a surprising finding of [6] and could already be understood on the basis of DFT calculations, see the discussion in [22]

and a forthcoming detailed paper. These new findings now answer all the open questions from [6] concerning the topology of the phase diagram of this 2D fluid with internal quantum states.

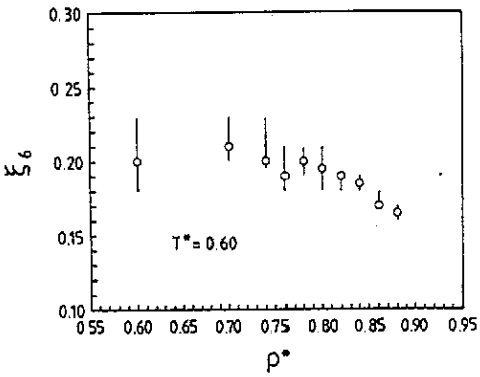

Figure 7. Fluctuation amplitude ξ_6 of hexagonal Γ_6 patterns as a function of ρ^* for $T^* = 0.6$.

In addition, we can supply in figure 7 the data for the optimized fluctuation amplitudes ξ_6 of the hexagonal patterns as a function of density for $T^* = 0.6$. Casting a quick glance at this figure, one notes that ξ_6 decreases as the density is increased. A more careful inspection reveals that ξ_6 stays (within the mutual error bars) constant up to ρ^*_{coex} and only then rapidly decreases for higher densities; the behaviour of ξ_6 for the other three temperatures is qualitatively the same. In addition, one can extract $\xi_6/\sqrt{2}$ at ρ^*_{coex} as a function of temperature. Ordered as $(T^*, \xi_6/\sqrt{2})$, these data read (0.45, 0.13), (0.6, 0.14), (1.0, 0.13), and (1.5, 0.14) with an estimated error of roughly ± 0.02. The Lindemann parameters as obtained from the DFT calculations for the liquid–hexagonal-solid transition are 0.14 at $T^* = 1.0$ and 0.15 at $T^* = 0.6$. This agreement again demonstrates that the decomposition of the overall density $\rho(Q, T^*, \rho^*)$ in hexagonal and defect patterns with different fluctuation amplitudes is justified and, moreover, contains very useful information in terms of c_6 and ξ_6.

Before coming to our conclusions, we want to discuss other recent approaches similar in spirit to ours. The analysis of [11] is devoted to the order–disorder transition in the hard-disk system. It is also based only on configurations; in this case it is the edge-length distribution function of the Voronoi polygons as obtained from a tesselation of the configurations. It was demonstrated that the distribution of this quantity can serve to give an estimate of the transition parameters in the hard-disk fluid. However, no direct comparison of the obtained transition pressure with other results was made, so that we cannot judge the quality of the Voronoi method as compared to our local structure analysis. In the investigation [18] of soft repulsive spheres, bond-order parameter distributions were also used, but the goal was to study free-energy barriers in crystal nucleation and not to locate any phase transition. Finally, the question of how to simulate and analyse an *equilibrium* solid without imposing any implicit constraints on the system is highly non-trivial, and is discussed in great detail in [28]. It is *not* sufficient to simulate in NpT or constant-stress ensembles in order to circumvent artificial constraints due to finite-sized systems and boundary conditions. In [28] a method is devised for reliably extracting thermodynamic data for *equilibrium* solids without imposing any artificial constraints due to the simulation of small systems. These authors introduce the 'bicanonical ensemble' and sophisticated methods for the analysis of necessarily a set of bicanonical simulations. The proposed method is very time consuming

since for each statepoint in the phase diagram several independent simulations and the evaluation of the free energy are required. Thus, though very accurate and promising, this approach is currently not practicable for investigations of phase transitions in many-body quantum systems as in our case.

6. Summary and conclusions

In the present investigation we combined the path-integral MC method for the simulation of many-body quantum systems with analysis techniques based on the properties of local real-space structures. Our model fluid, a 2D hard-disk fluid with internal quantum states, which is at the same time a prototype model for adsorbed molecular monolayers, is computationally very demanding, and only *efficient* analysis methods enable us to extract information on phase boundaries in this system. Such a method is devised by the local structure analysis based on 'fluctuating distributions' of *local* invariants. Using only a few configurations it is nevertheless possible to obtain reliable estimates of the liquid–hexagonal-solid transition density as a function of temperature. The numerical results compare favourably with a recent DFT calculation of the phase diagram. This demonstrates the usefulness and efficiency of the local structure analysis for the direct location of the liquid–solid coexistence line in simulations without having to rely on computations of thermodynamic functions. Again, we stress the point that the present study has a mainly exploratory character, and a detailed analysis of free energies based on much better statistics, larger systems and finite-size extrapolations is required in order to extract more accurate data. However, the local structure analysis method as presented in this study is tailored to a rough estimation of liquid–solid coexistence densities over a wide range of control parameters for computationally demanding fluid models.

In addition to these methodological aspects, we are now able to follow the liquid–hexagonal-solid coexistence line until it reaches the gas–liquid binodal. This shows by simulation that *two* triple points exist in the 2D hard-disk fluid with internal quantum states (associated with the *square* solid at very low temperatures and the usual *hexagonal* solid) as recently conjectured from a DFT treatment of this fluid. Thus, the topology of the phase diagram of this 2D fluid with internal quantum states can now be considered to be well understood.

Acknowledgments

It is a pleasure to thank K Binder and D Frenkel for useful discussions and comments. Most of the programs for the local structure analysis were developed during the stay of ACM at the Universität Saarbrücken as an Alexander von Humboldt Fellow. PN thanks the Deutsche Forschungsgemeinschaft for a Heisenberg fellowship and DM acknowledges his continuous support (Bi 314/5 and Forschungsstipendium). AZP thanks the Sonderforschungsbereich 237 'Unordnung und große Fluktuationen' for financial support. Finally, this work would have been impossible without grants of computer time on the Cray-YMP (HLRZ Jülich) and VP 100 (RHRK Kaiserslautern) vector processors.

References

[1] Levesque D, Weis J J and Hansen J P 1979 *Monte Carlo Methods in Statistical Physics* ed K Binder (Berlin: Springer) ch 2, p 47; 1984 *Applications of the Monte Carlo Methods in Statistical Physics* ed K Binder (Berlin: Springer) ch 2, p 37
Levesque D and Weis J J 1992 *Monte Carlo Methods in Condensed Matter Physics* ed K Binder (Berlin: Springer) ch 6, p 112

[2] Hoover W G and Ree F H 1967 *J. Chem. Phys.* **47** 4873

[3] Meijer E J and Frenkel D 1991 *J. Chem. Phys.* **94** 2269

[4] Panagiatopoulos A Z 1987 *Mol. Phys.* **61** 813; 1992 *Mol. Simul.* **9** 1
Smit B 1990 Simulation of phase coexistence: from atoms to surfactants *Proefschrift* Rijksuniversiteit Utrecht

[5] Rovere M, Heermann D W and Binder K 1988 *Europhys. Lett.* **6** 585; 1990 *J. Phys.: Condens. Matter* **2** 7009
Rovere M, Nielaba P and Binder K 1993 *Z. Phys.* B **90** 215

[6] Marx D, Nielaba P and Binder K 1991 *Phys. Rev. Lett.* **67** 3124; 1993 *Phys. Rev.* B **47** 7788
Marx D 1992 *Surf. Sci.* **272** 198

[7] Marx D 1993 *Computer Simulation Studies in Condensed Matter Physics VI* ed D L Landau, K K Mon and H B Schüttler (Berlin: Springer) at press

[8] Mezei M 1980 *Mol. Phys.* **40** 901; 1992 *Mol. Simul.* **9** 257
Ruff I, Baranyai A, Pálinkás G and Heinzinger K 1986 *J. Chem. Phys.* **85** 2169

[9] Tenemura M, Hiwatari Y, Matsuda H, Ogawa T, Ogita N and Ueda A 1977 *Prog. Theor. Phys.* **58** 1079

[10] Nosé S and Yonezawa F 1986 *J. Chem. Phys.* **84** 1803

[11] Fraser D P, Zuckermann M J and Mouritsen O G 1990 *Phys. Rev.* A **42** 3186; 1991 *Phys. Rev.* A **43** 6642

[12] Hess S 1980 *Z. Naturf.* a **35** 69

[13] Nelson D R and Toner J 1981 *Phys. Rev.* B **24** 363
Steinhardt P J, Nelson D R and Ronchetti M 1983 *Phys. Rev.* B **28** 784

[14] Mitus A C and Patashinskii A Z 1981 *Sov. Phys.–JETP* **53** 798; 1982 *Phys. Lett.* **87A** 179

[15] Mitus A C and Patashinskii A Z 1988 *Physica* A **158** 371; 1988 *Physica* A **158** 383

[16] Gades H and Mitus A C 1991 *Physica* A **176** 297

[17] Mitus A C, Patashinskii A Z and Sokolowskii S 1991 *Physica* A **174** 244

[18] van Duijneveldt J S and Frenkel D 1992 *J. Chem. Phys.* **96** 4655

[19] Strandburg K J 1988 *Rev. Mod. Phys.* **60** 161
Kleinert H 1989 *Gauge Fields in Condensed Matter* vol II (Singapore: World Scientific) part III, ch 14
Glaser M A and Clark N A *Adv. Chem. Phys.* at press

[20] Ballone P, de Smedt Ph, Lebowitz J L, Talbot J and Waisman E 1987 *Phys. Rev.* A **35** 942
de Smedt Ph, Nielaba P, Lebowitz J L, Talbot J and Dooms L 1988 *Phys. Rev.* A **38** 1381

[21] Strandburg K J, Zollweg J A and Chester G V 1984 *Phys. Rev.* B **30** 2755
Zollweg J A, Chester G V and Leung P W 1989 *Phys. Rev.* B **39** 9518

[22] Sengupta S, Marx D and Nielaba P 1992 *Europhys. Lett.* **20** 383

[23] Chandler D and Wolynes P G 1981 *J. Chem. Phys.* **74** 4078
Berne B J and Thirumalai D 1986 *Ann. Rev. Phys. Chem.* **37** 401
Chandler D 1991 *Liquids, Freezing and Glass Transition* ed J P Hansen, D Levesque and J Zinn-Justin (Amsterdam: Elsevier)
Schmidt K E and Ceperley D M 1992 *Monte Carlo Methods in Condensed Matter Physics* ed K Binder (Berlin: Springer)

[24] Frenkel D and McTague J P 1979 *Phys. Rev. Lett.* **42** 1632

[25] Stratt R M 1984 *J. Chem. Phys.* **80** 5764; 1984 *Phys. Rev. Lett.* **53** 1305
Desjardins S G and Stratt R M 1984 *J. Chem. Phys.* **81** 6232

[26] Stanley H E 1971 *Introduction to Phase Transitions and Critical Phenomena* (Oxford: Oxford University Press)

[27] Ramakrishnan T V and Yossouf M 1979 *Phys. Rev.* B **19** 2775
Haymet A D J and Oxtoby D J 1981 *J. Chem. Phys.* **74** 2559
For recent reviews see
Baus M 1990 *J. Phys.: Condens. Matter* **2** 2111
Oxtoby D W 1991 *Liquids Freezing and the Glass Transition—Les Houches Session LI* (Amsterdam: North-Holland)
Singh Y 1991 *Phys. Rep.* **207** 351

[28] Swope W and Andersen H C 1992 *Phys. Rev.* A **46** 4539
Andersen H C and Swope W *Preprint*